Journal of
*Manufacturing and Materials Processing*

MDPI

*Article*

# Microstructural and Mechanical Characterization of Ledeburitic AISI D2 Cold-Work Tool Steel in Semisolid Zones via Direct Partial Remelting Process

**M. N. Mohammed [1,*], M. Z. Omar [2], Adnan Naji Jameel Al-Tamimi [3], Hakim S. Sultan [4], Luay Hashem Abbud [5], Salah Al-Zubaidi [6], Oday I. Abdullah [7,8,9] and M. Abdulrazaq [10]**

[1] Mechanical Engineering Department, College of Engineering, Gulf University, Sanad 26489, Bahrain
[2] Department of Mechanical and Materials Engineering, Faculty of Engineering and Built Environment, Universiti Kebangsaan Malaysia, Bangi 43600, Malaysia
[3] College of Technical Engineering, Al-Farahidi University, Baghdad 10001, Iraq
[4] Department of Air-Conditioning and Refrigeration Techniques Engineering, University of Warith Al-Anbiyaa, Holy Karbala 56001, Iraq
[5] Air Conditioning and Refrigeration Techniques Engineering Department, Al-Mustaqbal University College, Babylon 51001, Iraq
[6] Department of Automated Manufacturing Engineering, Al-Khwarizmi College of Engineering, University of Baghdad, Baghdad 10071, Iraq
[7] Department of Energy Engineering, College of Engineering, University of Baghdad, Baghdad 10071, Iraq
[8] System Technologies and Engineering Design Methodology, Hamburg University of Technology, 21073 Hamburg, Germany
[9] Department of Mechanics, Al-Farabi Kazakh National University, Almaty 050040, Kazakhstan
[10] Research Center, The University of Mashreq, Baghdad 10023, Iraq
* Correspondence: dr.mohammed.alshekhly@gulfuniversity.edu.bh; Tel.: +973-37435993

**Abstract:** The success of the thixoforming process largely depends on the created microstructure, which must be globular in the liquid phase. The solid–liquid structural changes that occur on as-annealed D2 tool steel when it is subjected to the so-called DPRM are described in this work (direct partial remelting method). The paper discusses phase changes and how carbide dissolution affects grain boundary liquation and grain spheroidization. Equiaxed grains with undissolved carbide particles have been found in the microstructural analysis at 1250 °C; however, the carbides gradually disappear as the temperature rises. Additionally, the equiaxed grains were transformed to a globular structure, which improves the shape factor and grain size for the thixoforming process. For AISI D2 thixoforming, which produced grains with a diameter of 50 µm and a shape factor of 1.18, temperatures of 1300 °C and a holding period of 5 min were the optimum parameters. The outcomes also showed that the mechanical properties of the AISI D2 were greatly enhanced after using direct partial remelting, where hardness was increased from 220 Hv to 350 Hv and tensile strength from 791 MPa to 961 MPa.

**Keywords:** thixoforming; semisolid metal processing; AISI D2 tool steel; direct partial remelting; spherical morphologies

check for updates

**Citation:** Mohammed, M.N.; Omar, M.Z.; Jameel Al-Tamimi, A.N.; Sultan, H.S.; Abbud, L.H.; Al-Zubaidi, S.; Abdullah, O.I.; Abdulrazaq, M. Microstructural and Mechanical Characterization of Ledeburitic AISI D2 Cold-Work Tool Steel in Semisolid Zones via Direct Partial Remelting Process. *J. Manuf. Mater. Process.* **2023**, *7*, 11. https://doi.org/10.3390/jmmp7010011

Academic Editor: Steven Y. Liang

Received: 4 November 2022
Revised: 12 December 2022
Accepted: 20 December 2022
Published: 28 December 2022



## 1. Introduction

AISI D2 tool steel is commonly utilized cold-work steel which it is rich in carbon and chromium. It is characterized by numerous mechanical and tribological characteristics such as high deep hardenability, excellent wear resistance, and compressive strength that makes it suitable for a wide range of usages, such as blanking dies, punches, and mill rolls. However, the forming of this type of steel by traditional forging and casting consumes high energy and takes a lot of time [1]. Thus, demands for a new method that can minimize energy consumption and the production cycle and replace the classical process is really required. After the published study of Spencer et al. in 1972 [2], who defined the principle of

thixotropic behavior, the semisolid processing technology received significant consideration in the world due to the capability to improve and facilitate the production with high quality and reasonable cost when it is compared with traditional casting or forging. For example, the quality of the finished product is improved by semisolid processing compared to casting due to the reduction in defects that are introduced during solidification. In addition, intricate shapes can be obtained and produced to near-net-shape in a single operation with good mechanical properties due to low forming loads, compared to the forging process [3]. Generally, thixoforming process depends on the melting range and working windows, which must be cognizable and sufficiently large [4]. The successful process demands billet or stock consisting of globular and fine solid particles dispersed within a liquid matrix in order to achieve thixotropic behavior [5]. Up to this point, low-meltingpoint alloys such as aluminium and magnesium alloys, receive major concern from researchers for processing by the semisolid method (SSM) [6]. High-temperature materials, including steel, cast iron, composites, and copper-based alloys, also receive considerable interest from researchers for processing by the semisolid route [7–9]. However, the thixoforming of Fe-based alloys has not been realized industrially due to the high working temperature, potential for surface oxidation, and complicated microstructural evolution during semisolid forming, which means that the requirements for the starting material are quite stringent [10]. Nevertheless, investigators are becoming more attracted to and interested in this research area because of steel thixoforming merits. Several steel grades such as HP9430 [11], X210CrW12 [12], 100Cr6 [13], SKD61 [14], 304 [15], M2 steels [16–20] have already been evaluated with respect to their suitability for the thixoforming process.

Several processing routes that were utilized for the production of non-dendritic feedstocks as candidate materials for semisolid processing are reviewed comprehensively in [21]. According to Omar et. al. 2008 [16], direct partial remelting (DPRM) is considered a lab-friendly process that requires little apparatus and equipment. This innovative technology can be used to directly reheat an alloy as received between solidus and liquidus (semisolid range) without the need for common raw material preparation methods, such as the melt-activated and stress-induced routes, the partial melting method, and others [16]. This suggests that there is the potential to increase the range of routes available for the production of thixoformable microstructures. During semisolid cooling, M2 steel underwent intragranular acicular ferrite (IAF) transformation at a very high temperature (1180 960 °C) [21]. Using a confocal laser scanning microscope, the unusual IAF change was seen in action. Tiny VC carbide particles formed, largely during semisolid cooling, and acted as the favored site for the IAF nucleation due to the minimum lattice mismatch with ferrite. The bimodal trend of the ferrite lath length indicates that long primary and secondary ferrite laths coexisted. The solid border or interface was where the acicular laths intersected and came to an end. The acicular ferrite covered the previously solid austenite grain. The IAF could assist in increasing the strength of semisolid M2 steel by reducing the effective grain size.

The processability and deformability of the three semisolid high-entropy alloys ($CoCrCu_1FeNi$, $CoCrCu_2FeNi$, and $CoCrCu_3FeNi$) were investigated by Chaussê de Freitas et al. [18]. Because of its crucial role in the liquid fraction, the Cu content at 1175 °C significantly impacted the semisolid's deformation. The alloys that were semisolid showed a feature of pseudoplastic rheology. It is found that only the $CoCrCu_3FeNi$ alloy completely filled the die during thixoforming. The Vickers hardness decreased as the Cu content increased as a result of the different hardness values of the individual FCC phases. The compression test findings showed that the thixoformed $CoCrCu_3FeNi$ had a yield stress of 310 MPa and high plasticity. Semisolid processing is thus an alternative method of producing parts made up of high-entropy alloys.

Chaussê de Freitas et al. [19] conducted a review study regarding the assessment criteria for the processability of semisolid processed alloys. They found that there are three adopted criteria to evaluate the semisolid processability. The temperature was the

most commonly adopted parameter while time had large adaptability, and finally, enthalpy seems more reasonable.

Jirková et al. [22] studied the semisolid parameter of X210Cr12 tool steel. The tool steel was quenched in oil or water from the semisolid zone (1200 °C to 1280 °C) and formed in a press. The process achieved the successful removing of primary Cr-carbides. The produced microstructure consisted of around 1 µm martensite + austenite matrix with fine $Cr_7C_3$ and $Fe_3C$ carbides.

Meengam and Sillapasa [23] examined the response of AA 6063 alloy in semisolid conditions to the friction stir welding process. Factorial design assisted with ANOVA was adopted to discuss the impact of rotational and welding speeds beside tool geometry on the tensile strength. The optimum parameters, namely, 1300–2100 rotational speed, less than 75 mm/min welding speed, and cylindrical pin, have produced 120.7 MPa as tensile strength. SEM and EDS results revealed new recrystallized grains in thermo-mechanically affected zones: coarse grains in the advanced side, and equiaxed grains in the retracing side.

Nakowong and Sillapasa [24] investigated the friction stir weldability of semisolid processed AA 5083 aluminum alloy. The achieved tensile strength, hardness and microstructure were analyzed according to ANOVA. The process parameters were optimized by using the Taguchi method. The rotational and travel speeds of 1000 rpm, 10 mm/min, with a cylindrical tool having a threaded profile, maintained a tensile strength of 235.22 Mpa. Meanwhile, the microhardness of 80.64 Hv was achieved at optimum settings of both speeds (1200 rpm ad 10 mm/min) with the threaded cylindrical pin. The rotational speed greatly influences the tensile strength, while no high-parameter influence was recorded for hardness. SEM and EDS tests revealed elongated grains with some voids located at the tip of the pin.

Due to some difficulties associated with the semisolid processing of X210Cr12 to steel, Paixão Ritter and Tempel Stumpf [25] applied FEM to simulate the semisolid processing to eliminate the possible errors that may accompany the real processing. The steel samples were simulated under hot compression conditions. A real experiment was taken for comparison with numerical findings. The proposed FEM model was suited for the evaluation of the semisolid processing of tool steel.

The mechanisms of deformation during direct partial remelting of AA 7075 were studied by Wang et al. [26]. The findings revealed simultaneous inter- and intragranular deformation during the semisolid extrusion process. The shrinkage of intergranular liquid was compensated by the deformed solid primary alpha phase. The sub-grain boundaries were induced by the change of globular grain morphology as a result of intragranular deformation at the end of semisolid processing.

The current study is an extension to the published work [20] and involves deep analyses for the identified evolved microstructures, liquid fraction, and mechanical properties. Also, the evolution of as-annealed ledeburitic AISI D2 tool steel to the non-dendritic microstructure during partial remelting was studied. In particular, the phase transformations and the effect of carbide dissolution on grain boundary liquation and grain spheroidization prior to thixoforming were investigated.

## 2. Experimental Procedure

AISI D2 is a ledeburitic steel with a high chromium content devoted to tools used in forming. It is characterized as being difficult to form and machine with conventional technologies. The initial as-received material was provided as-annealed through heating up to 850 °C followed by air cooling to 650 °C at a 10 °C/h rate. The chemical constitution of the obtained material was ascertained using the X-ray fluorescence (XRF) method, as shown in Table 1. The phase diagram of AISI D2 tool steel is shown in Figure 1.

**Table 1.** The XRF florescence compositional analysis of D2 cold-work tool steel.

| Element | Experimental | Nominal (ASM 1998) |
|---|---|---|
| C | 1.55 | 1.4–1.6 |
| Si | 0.258 | 0.6 (max) |
| Mn | 0.239 | 0.6 (max) |
| P | 0.025 | |
| S | 0.01 | |
| Cr | 11.2 | 11–13 |
| Ni | 0.197 | 0.3 (max) |
| Mo | 0.79 | 0.7–1.2 |
| V | 0.85 | 1.1 (max) |
| W | 0.2 | |
| Cu | 0.08 | |
| Fe | Balance | Balance |

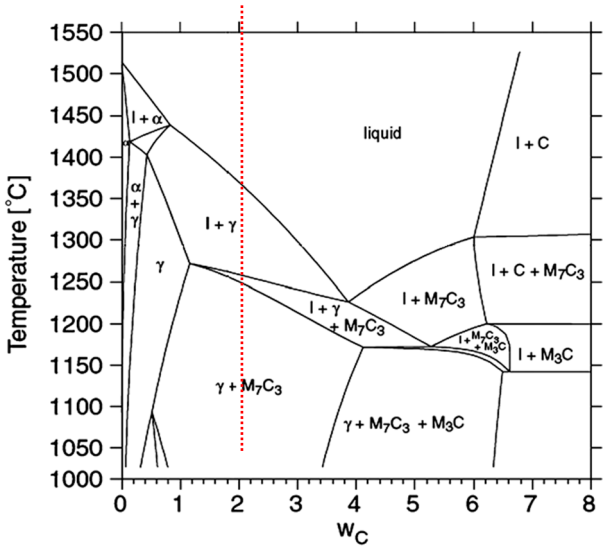


**Figure 1.** Phase diagram of AISI D2 tool steel [12].

A useful software package called Java-based material properties (JMatPro) was adopted to perform some important thermodynamic analyses. It involves various theoretical models for materials and their property database, enabling quantitative computing of the necessary material properties that can be performed over a larger software structure [21]. For D2 tool steel, the liquid fraction profile (LFP) and solidus and liquidus temperatures are calculated using the JMatPro software. The software calculations are performed through thermodynamic modeling of an equilibrium solidification that enables estimating and predicting different materials' critical physical and thermophysical points. The liquidus and solidus temperatures and liquid fraction were calculated by utilizing analysis of differential scanning calorimetry (DSC) in the semisolid zone. The material was tested by a Netzsch-STA 449 F3 simultaneous thermogravimeter utilizing small specimens (less than 20 mg) of the as-received material (TGA–DSC). For the purpose of preventing oxidation, the specimens were heated at a rate of 10 °C/min in a nitrogen environment. The estimation of liquid fraction was determined by analyzing the partial integral area underneath the endothermic diagram. The releasing or consuming of energy on the heating curve is indicative of phase transformation. The amount of discrepancy is related to the quantity of phase. Each peak's temperatures were identified, and the variations corresponding to particular peaks were confirmed.

As depicted, a high-temperature vertical carbolite furnace protected with argon gas was used to conduct the DPRM experiment. The diameter and length of the samples that

were cut from the original material are 16 mm and 100 mm, respectively. Once the moment that furnace reached the pre-selected temperature (1250, 1275, and 1300 °C), the sample was dropped into the furnace by using chromehromel wire for 5 min before being cooled slowly at room temperature as shown in Figure 2. Figure 3 shows the thermal cycle of DPRM process.

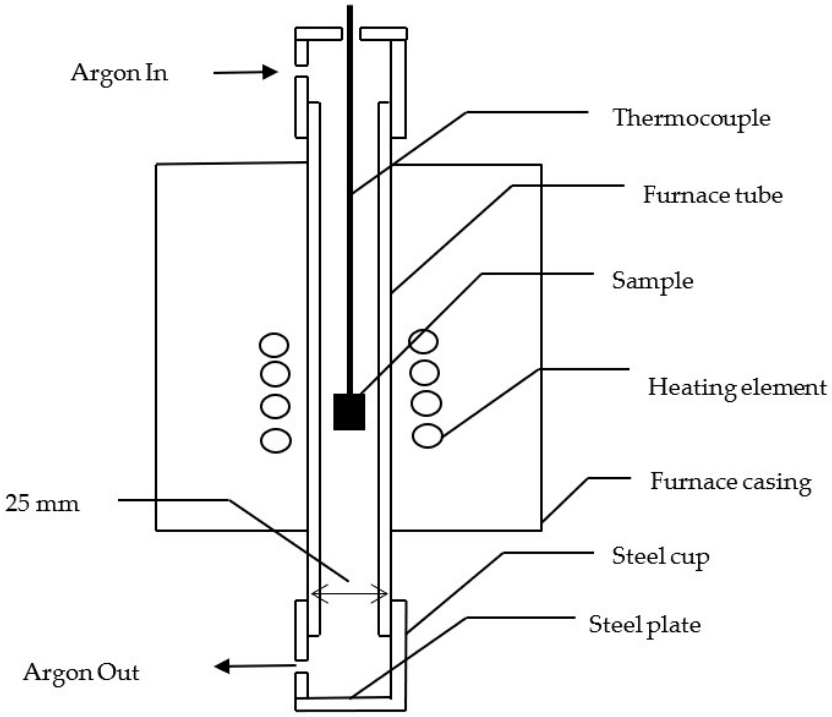


**Figure 2.** Schematic furnace set-up of direct partial remelting process.

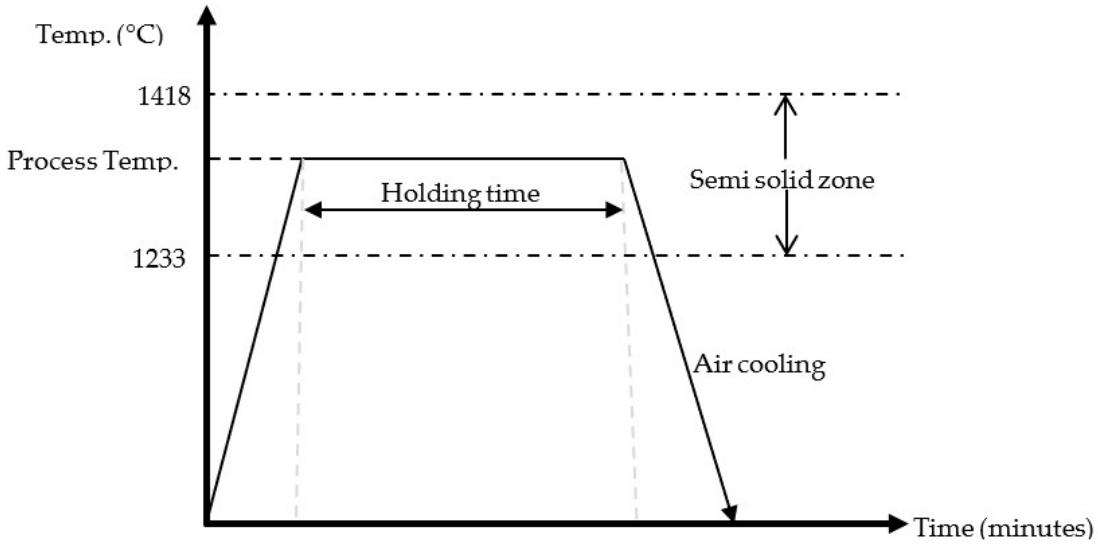


**Figure 3.** Temperature profile of sample inside vertical tube furnace.

A Hitachi S3400N scanning electron microscope (SEM) with energy dispersive spectroscopy (EDS) and an Olympus BX-51 optical microscope were used for microstructural characterization. An X-ray phase analysis was carried out to determine the evolved phases and different forms of carbides. The size and shape of the grains were quantitatively determined using ImageJ software. $P^2/4A$, where P represents the particle's perimeter and A its area, was used to define the shape factor. Thus, a circle has a shape factor of 1, and

its grains are totally spherical, whereas a more complicated shape might be created with a shape factor higher than 1. Given that $A_i$ is the area of each particle and N is the total number of particles in each image, the average size of the primary particles was calculated as $[\sum 2 (A_i/\pi)^{1/2}]/N$. Based on the recommendations of Hirt et al. [27], the suitable grain size and shape factor of the semisolid part must not exceed 100 μm and 2, respectively. All specimens have been etched using Villela reagent (picric acid (1 g), hydrochloric acid (5 mL) and ethyl alcohol (95 mL)) for microstructure examination. The Vickers hardness (HV) and tensile tests determined the mechanical characterization. A load of 2 kg was applied in the hardness test for 15 s. The Zwick universal testing machine was used to carry out the tensile test at room temperature to determine the ultimate tensile strength (UTS) and construct the stress–strain diagram. Then, each sample was cut into smaller pieces to be ready for metallographic examination. The pieces were examined using a TM-1000 microscope which operates at 15 kV with (100–5000×) magnification range. The process flow for this experimental procedure is shown in Figure 4.

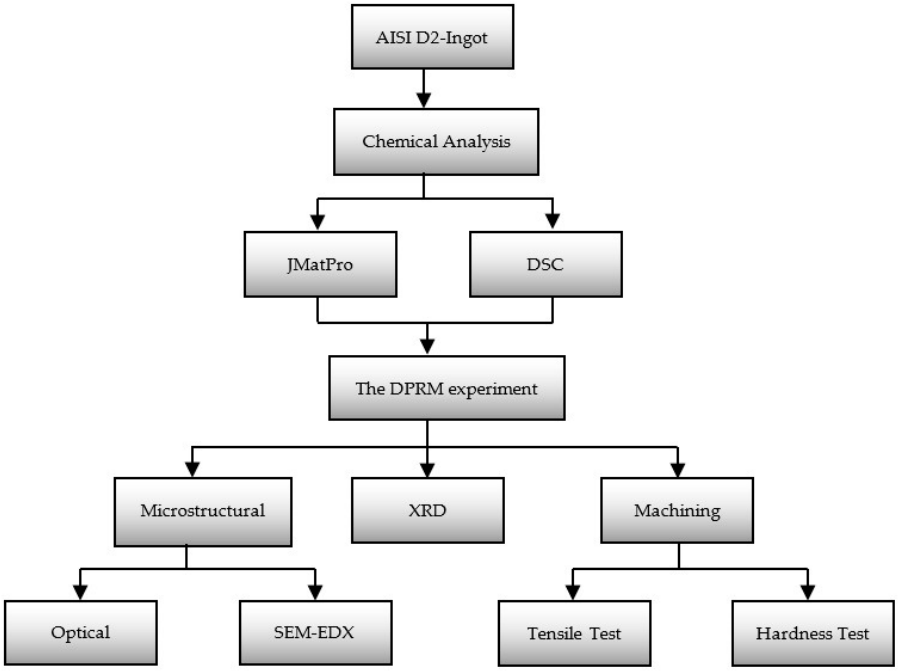


**Figure 4.** Process flow of the experimental procedure.

## 3. Results and Discussion

### *3.1. Liquid Fraction Profile and Transformations of Phases*

#### 3.1.1. Thermodynamic Modelling Using JMatPro

Figure 5 depicts the AISI D2 equilibrium phase diagram that was calculated using the JMatPro thermodynamic modelling package. It displays the phase changes of austenite, ferrite, and liquid between 0 °C and 600 °C, as well as carbides (MC, $M_7C_3$, and $M_{23}C_6$). It should be noted that JMatPro modelling is performed when the metal is in the equilibrium state to ensure that the actual condition of the structure can be determined and observed.

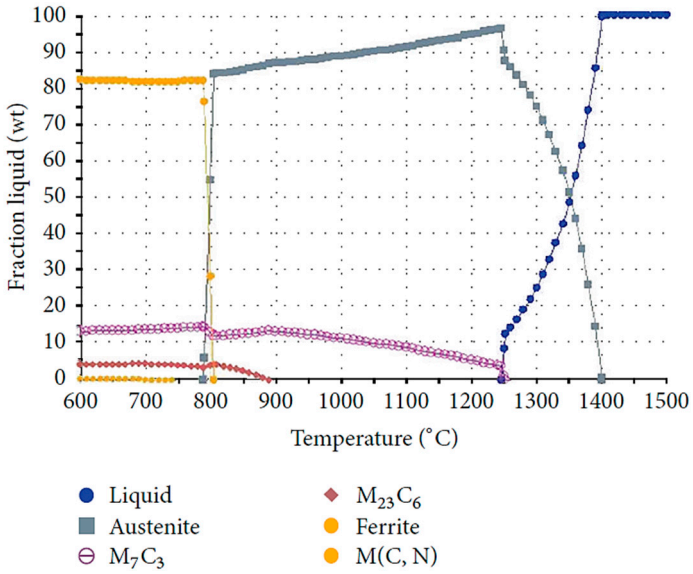


**Figure 5.** AISI D2 tool steel equilibrium phase diagram generated by JMatPro simulation.

It predicts the solidus temperature of approximately 1220 °C and liquidus at 1400 °C, respectively. The austenite phase begins to emerge at 790 °C and is predicted to dissolve completely at 1400 °C, as indicated by the liquidus temperature. The critical part of the process occurs at a temperature of 790 °C. At this temperature, $M_7C_3$ carbides exist (at 13–14% volume). This is also the case for MC carbides (at 0–2% volume). It is only when reheating, starting from room temperature, and before reaching the critical temperature, that these carbides dissolve completely at a temperature of 740 °C. Above the critical temperature, the amount of $M_7C_3$ carbides decreases gradually, then completely dissolves at 1251 °C, or in other words, these carbides are located within the zone of semisolid. As for the $M_{23}C_6$ carbides, these dissolve completely at 889 °C while the stability zone is being established between 170–889 °C. The chemical composition determined by JMatPro modelling was compared with the results of the dispersed energy spectroscopy test (as discussed in phase identification part). It should be noted that only the $M_7C_3$ carbides can be compared because the presence of $M_{23}C_6$ carbides is relatively small; in effect, it can be said that $M_{23}C_6$ carbides do not exist at room temperature in the simulation model. JMatPro modelling results are useful indicators for alloy systems under equilibrium conditions. However, there was precipitation of many estimated carbides, as the real case study is far from the equilibrium condition [28].

#### 3.1.2. Differential Scanning Calorimetry

The TGA–DSC apparatus was employed to analyze the phase transformation of the AISI D2 steel. As stated in the preceding section, phase changes are identified on the DSC curve based on a deviation that refers to energy fluctuation (consume or release) and the level of deviation determines the quantity of phases. Every peak with a corresponding temperature is defined and the varieties that are proportional to some peaks were verified. The temperatures of each peak were defined, and the changes proportionate to certain peaks were verified. The DSC heating curve, obtained using a 10 °C/min heating rate for the as-received steel, is shown in Figure 6.

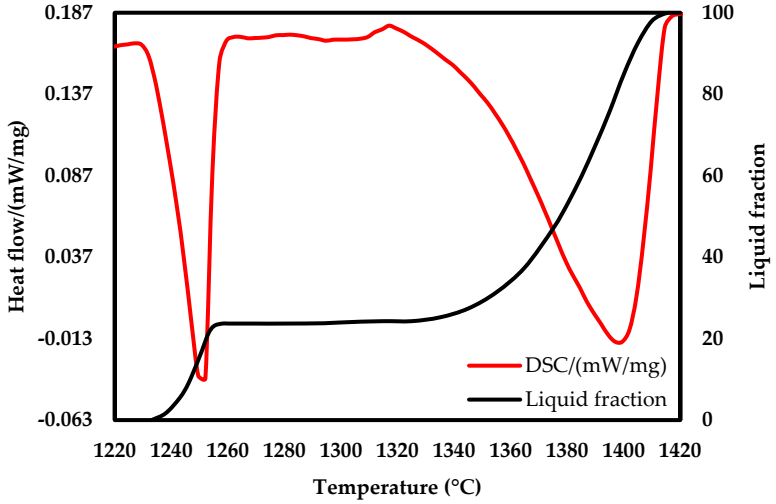


**Figure 6.** Differential scanning calorimetry liquid fraction and heating flow curves of D2 tool steel.

The start of the endothermic peak is considered the melting point, and this temperature is where melting begins to occur. The melting end is determined by the starting point on the other side of the peak as the heat curve deviates from the tangent line. At 1233 °C, the endothermic effect began, and at 1418 °C, it terminated. Using a "common tangent" method, the baseline for estimating the liquid fraction was created. Thus, the overall temperature difference between solidus and liquidus is 185 °C. This indicates that this type of steel has a large semisolid interval at relatively low-temperature sensitivity. For this reason, the percentage of liquid in this grade of steel is less sensitive and less affected by temperature change. The profile of the liquid fraction at low-temperature sensitivity is near to a straight horizontal line. Consequently, the temperature range is specified as 1250 °C and 1340 °C regarding the low sensitivity region.

Before focusing specifically on the influences of heat treatment, it is crucial to remember that the curves produced with low heating rates match those obtained with JMatPro at equilibrium conditions. The DSC heating curve reveals four main endothermic peaks which were produced due to transformation reactions associated with the dissolution of phases (Figure 7). The first visible change in the DSC heating curve is observable at 765 °C and is called the "Curie point". This peak corresponds to a transformation from the ferromagnetic to the paramagnetic state. The second peak indicates the ferrite/martensite transformation to austenite. There are two peaks in the melting interval, the first of which is associated with carbide dissolution and the second with complete austenite melting.

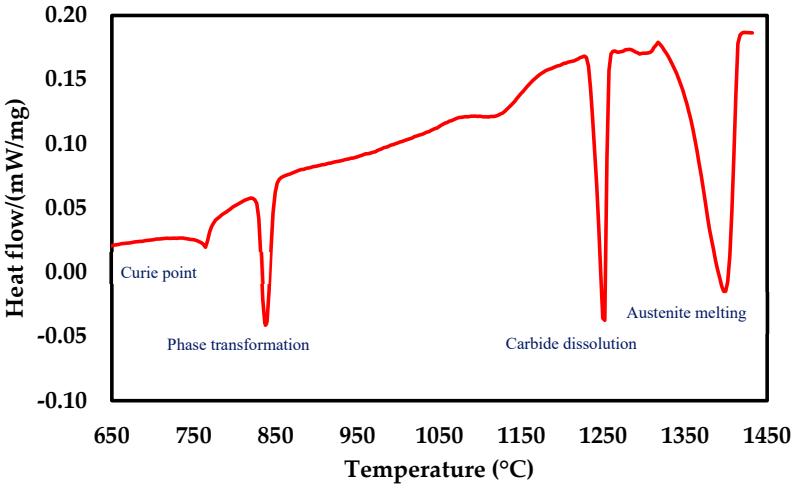


**Figure 7.** The DSC curve of D2 tool steel.

The equilibrium calculations of JMatPro were found to be acceptable estimations of the solidus temperatures for D2 tool steel when compared to those obtained experimentally from DSC. However, the quantity of liquid formed was underestimated by DSC compared to the equilibrium (e.g., at 1340 °C); the liquid fraction is around 43% and 25% by equilibrium and DSC, respectively). A possible explanation could be that, during heating under a non-equilibrium condition to above its solidus temperature, the solid composition does not have enough time to reach equilibrium; instead, the solid composition remains below 1420 °C and hence the amount of liquid formed is less than that which would be expected at equilibrium [16].

### *3.2. Structural Investigations*

Possibly the most critical step in the thixoforming process is the reheating of the billet prior to the forming stage. At this point in the process, the billet not only has to obtain the desirable nominal liquid fraction but also its microstructure should consist of a solid phase already transformed into ideally spheroidal solid particles or grains. The microstructural responses of the as-received D2 tool steel to experimental isothermal reheating into the semisolid state (1250 °C, 1275 °C and 1300 °C) and then held for 5 min at these temperatures are shown in Figure 8.

The microstructure of as-received D2 includes a ferritic matrix allocated parallel to the working direction with largely surplus carbides and uniformly distributed and spheroidal small carbides as displayed in Figure 8a. The microstructure examination confirmed the as-annealed conditions of this type of steel [16] and certainly affirmed that heat treatment was completed according to supplier recommendations.

At 1250 °C the equiaxed grains of austenite in the background became clearer within fewer entrapped liquid phases without a uniform orientation, and had recorded 70 µm grain size and 1.56 shape factor, as shown in Figure 8b. The microstructure has two types of carbides, namely, primary $M_7C_3$ undissolved carbides and new re-precipitated eutectic carbides which formed along grain boundaries during solidification. Also, at this temperature and according to the DSC profile in Figure 6, the liquid phase must be revealed at a volume fraction of 15%. However, microstructural observation revealed that a high amount of non-dissolved carbides was still present at this temperature. This is most probably because this temperature is not sufficient to dissolve the carbides in the steel. Hence, the carbide particles still existed in bands formed parallel to the working direction (longitudinal direction is in the vertical direction), as they also existed in the alloy in its as-supplied condition.

At a higher temperature, i.e., 1275 °C (23% liquid fraction), the existence of a liquid phase as well as diffusion mechanisms promote the wettability of the primary phase, which results in the transformation of grain morphology from equiaxed to relatively globular grain size of 61 µm and 1.3 shape factor, as shown in Figure 8c. Further heating dissolved all the remaining $M_7C_3$ carbides and increased the liquid fraction of eutectic carbides (the dark part of the Figure 8). Moreover, the austenite grains, which exhibited a relatively globular shape, were filled up and bounded by eutectic carbides that precipitated in the lamellar structure and also on grain boundaries.

A further temperature increase to 1300 °C (25% liquid fraction) led to the grain morphology exhibiting a fine spherical austenite primary phase after reheating. In this case, the carbide dissolution assists the globular transformation of grains, as depicted in Figure 8d. The carbide dissolution is advantageous due to the enlargement of the semisolid zone and lowering of temperature sensitivity [16]. Therefore, as isothermal heating temperature increases, the liquid phase begins to distribute along the grain boundaries and disperse more equally to produce globular grain. Spherical-shaped grains are considered as essential requirement for successful thixoforming [29–31]. The microstructures revealed that the thick liquid phase has separated the grains from each other. With enough wetting around the grain boundary, the grains start to flow past each other by shear during forming due to the thixotropic behavior of the slurry. With a grain size of 50 µm and a shape factor of 1.18,

spherical grains were well-arranged in a eutectic mixture, according to microstructural analysis. The microstructure development progressed with the particle size decreasing from 70 to 50 µm. Consequently, the globularity level increased by decreasing the shape factor from 1.56 to 1.18. Meanwhile, there was grain size reduction from 70 to 50 µm that facilitated the grain roundness as displayed in Figure 9. At the same time, the change in grain globularity with isothermal heating temperature took place synchronously with the grain size change.

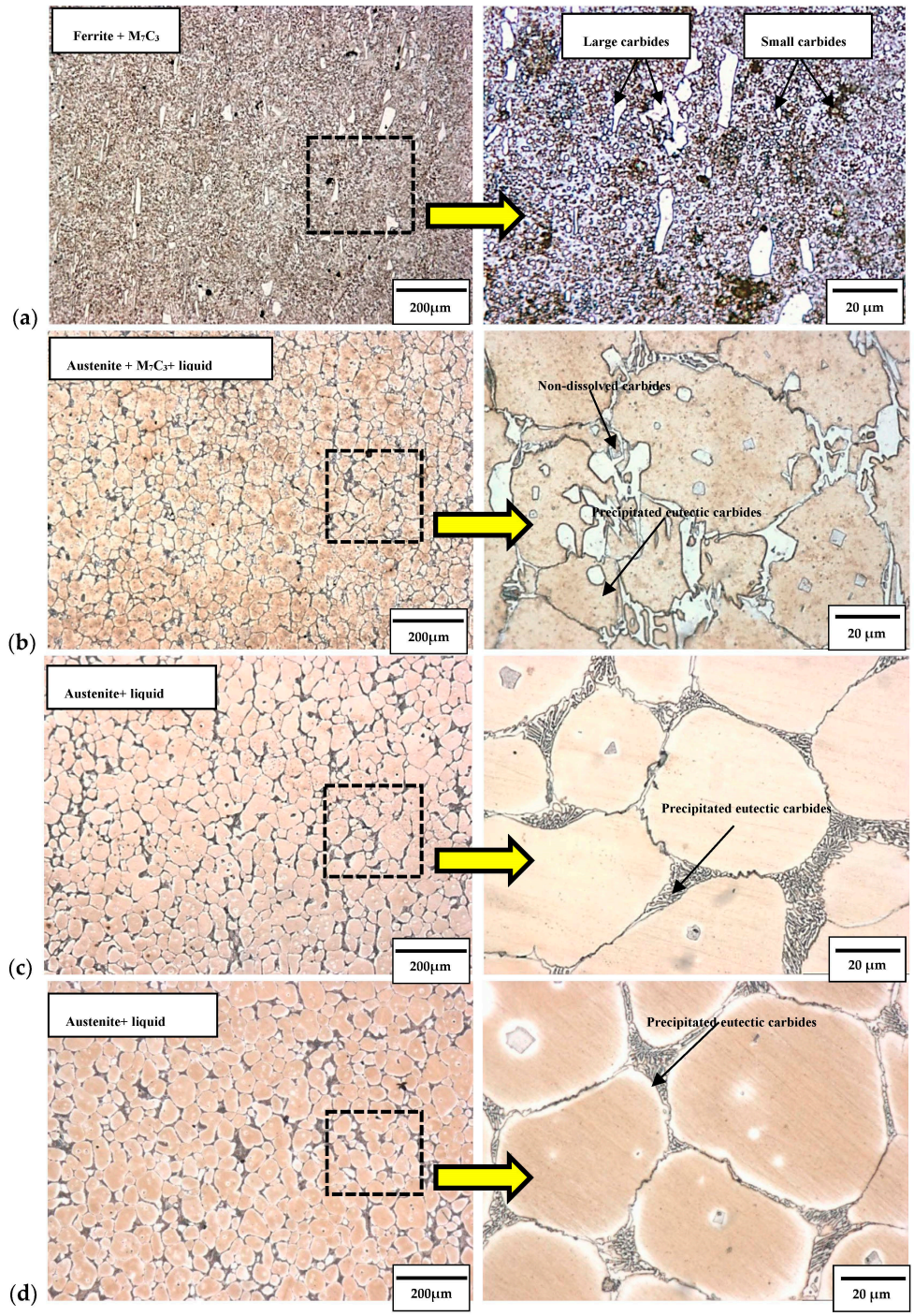


**Figure 8.** Optical micrographs of AISI D2 sample at (**a**) room temperature as received, (**b**) 1250 °C, (**c**) 1275 °C and (**d**) 1300 °C with holding time of 5 min.

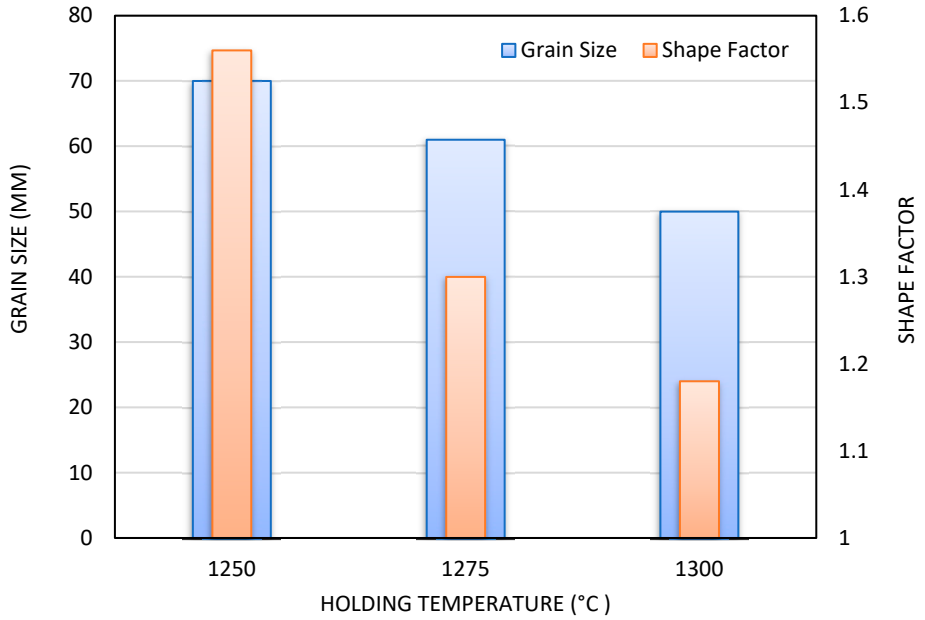


**Figure 9.** Differences in shape factor and the primary grain at 1250, 1275 and 1300 °C with 5 min holding time.

Therewith, most of the original carbides were dissolved with the increase in heating temperature, while new eutectic carbides were re-precipitated along grain boundaries during subsequent cooling by diffusing of carbide-forming elements into the grain boundaries. Hence, the penetration of liquid towards grain boundaries is facilitated and promoted with a high eutectic volume fraction [32]. The above discussion shows that the carbides influence the size and shape of the spheroidal structures in the microstructural development sequence for various temperatures above the solidus up to 1300 °C. For the purposes of this research, 5 min was chosen as holding time to enable the heated samples to approach the equilibrium status.

Posteriorly, melting and solidification in negative curvature zones are due to subsequent diffusion operations, resulting in the formation of solid particles of near-spherical shape inside the liquid matrix. In addition, reheating into the semisolid region during DPRM gives sufficient energy for the grain boundaries of the recrystallized structure to grow, while the presence of carbides prevents excessive grain size [33]. However, the presence of carbides prevents excessive grain size, as shown by the experimental results above, where grain sizes of 50 μm were produced. The achieved results so far prove that AISI D2 cold-work tool steel is a suitable candidate material for semisolid processing by DPRM from as-received condition and there is no necessity to prepare feedstock by traditional routes such as SIMA and RAP as summed up in Figure 10. This refers to a wide range of effective routes that can produce thixoformable microstructures.

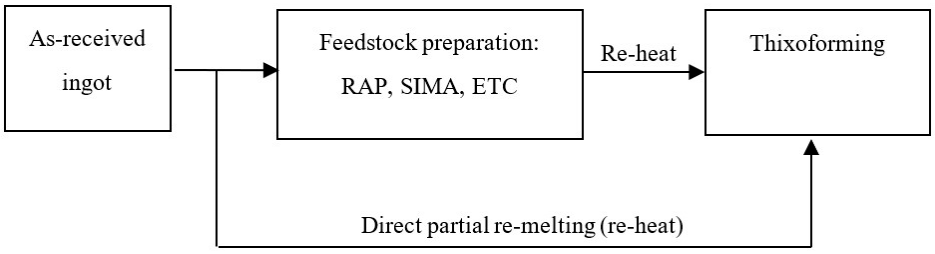


**Figure 10.** Various processing routes to acquire thixoformed structure.

### 3.3. Phase Identification

The received AISI D2 tool steel was supplied as-annealed and its microstructure consists of dispersed large and small carbides within the ferritic matrix as SEM revealed in Figure 11. Table 2 shows the compositional analysis of the carbides and ferrite matrix as determined by EDX. The $M_7C_3$ carbides can be noted, which are consisted mostly of C, Cr, and V, and that there are also carbides of type $M_{23}C_6$ that are rich in C, Cr and W. The MC carbides are dissolved at 740 °C, therefore, the as-received microstructure of AISI D2 tool steel was free from MC carbides due to soft annealing at 850 °C. Compared to $M_7C_3$ carbides, the amount of $M_{23}C_6$ carbides was insignificant after cooling to room temperature. The origin of the banded structures in the as-received D2 was verified by qualitative SEM-EDX elemental mapping, as shown in Figure 12. The representative concentration profiles of the elements considered in the analysis were Cr, V, C, and Fe; thus, it can be deduced that there is an increased carbide content, which conforms to the EDX results shown in Table 2.

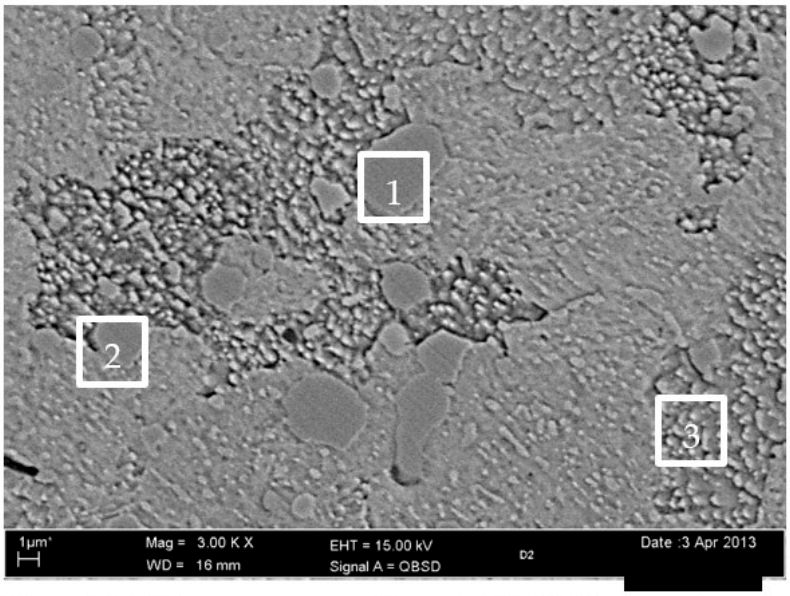


**Figure 11.** SEM microstructure of supplied AISI D2 tool steel.

**Table 2.** Compositional analysis of ferritic matrix and carbides as determined by EDX analysis.

| | C | Si | Mn | P | S | V | Mo | W | Ni | Cr | Fe | Phase |
|---|---|---|---|---|---|---|---|---|---|---|---|---|
| Pt 1 | 6.03 | 0.1 | 0.34 | 0.08 | 0.03 | 5.07 | 1.46 | 0.29 | 0.07 | 45.95 | 40.58 | $M_7C_3$ |
| Pt 2 | 6.70 | 0.16 | 0.49 | 0.02 | 0.24 | 5.52 | 1.57 | 0.10 | 0.09 | 44.51 | 40.62 | $M_7C_3$ |
| Pt 3 | 1.61 | 0.27 | 0.35 | 0.02 | 0.02 | 0.3 | 0.29 | 0.45 | 0.29 | 9.2 | 87.20 | α |

The phase diagrams (Figure 5) show the following during the heating phase before the forming process of high chromium steels, with regard to the enhancement of the structure at high temperatures over and just beneath the solidus line: (1) At 1300 °C, the liquid fraction is at the necessary level of around 25%, and the predominant solid phase is FCC austenite; (2) when the temperature is lowered below 1300 °C, the remaining liquid initially transforms into eutectic, ($L \rightarrow \gamma + M_7C_3$). It is widely known that the presence of alloying elements in the material, particularly carbon and chromium, determines the stability of austenite against martensitic transition at lower temperatures [29].

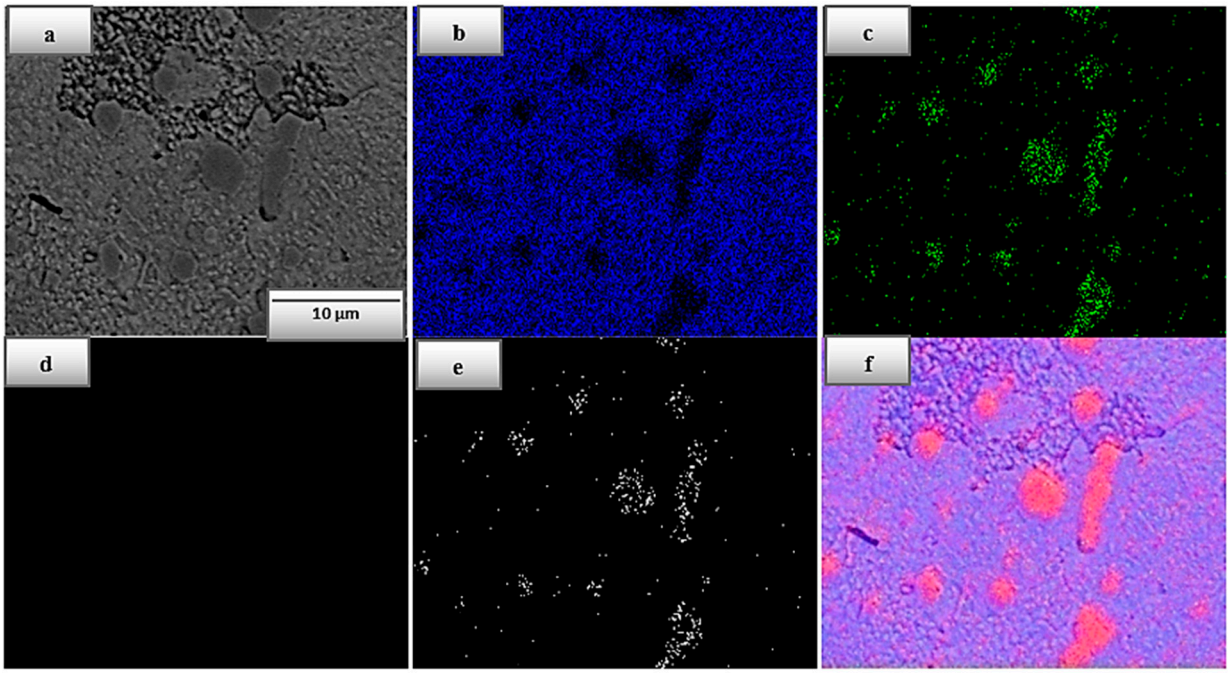


**Figure 12.** Elemental mapping of SEM-EDX for as-received D2 tool steel (**a**) SEM micrograph, (**b**) Fe, (**c**) Cr, (**d**) C, (**e**) V and (**f**) all four elements.

The start temperature of martensite is described as a function of C, Cr, Mo, Ni, and Mn in the austenite as given by Bhadeshia et al., 2006 [33]. These calculations revealed that the martensite begins to transform at −269 °C. The range of semisolid processing suggests that the austenite phase will be more stable at room temperature. Metastable austenite transformation contributes to the enhancement of the thixoforming properties of the material.

$$M_s \text{ Temp. } (^\circ C) = 539\text{-}423C\text{-}30.4Mn\text{-}17.7Ni\text{-}12.1Cr\text{-}7.5Mo \quad (1)$$

SEM analysis coupled EDX and EDS analyses and scanning electron microscopy were used to examine the phases that took place during the DPRM process. Figure 13 illustrates the EDX analysis results for points 1 and 2 of the SEM image. Point 1 is evidence of the presence the metastable austenite phase as indicated by EDX analysis. While re-formed eutectic carbides filled up the remained interspaces, grain boundaries and lamellar structure. Therefore, point 2 of the eutectic area was rich with C, Cr, and V [34]. SEM-EDX elemental mapping methods were employed to provide a more thorough understanding of the microstructure. Based on element distribution, it can be inferred that Fe is localized specifically in the globular grains. A high presence of carbides is indicated by an increased content of V, C, and Cr, which are distributed uniformly on the boundaries of the globular grains (eutectic zone), as shown in Figure 14. This figure shows how the morphologies and compositions of the post-treatment samples differ significantly from those of the samples as received (Figure 11).

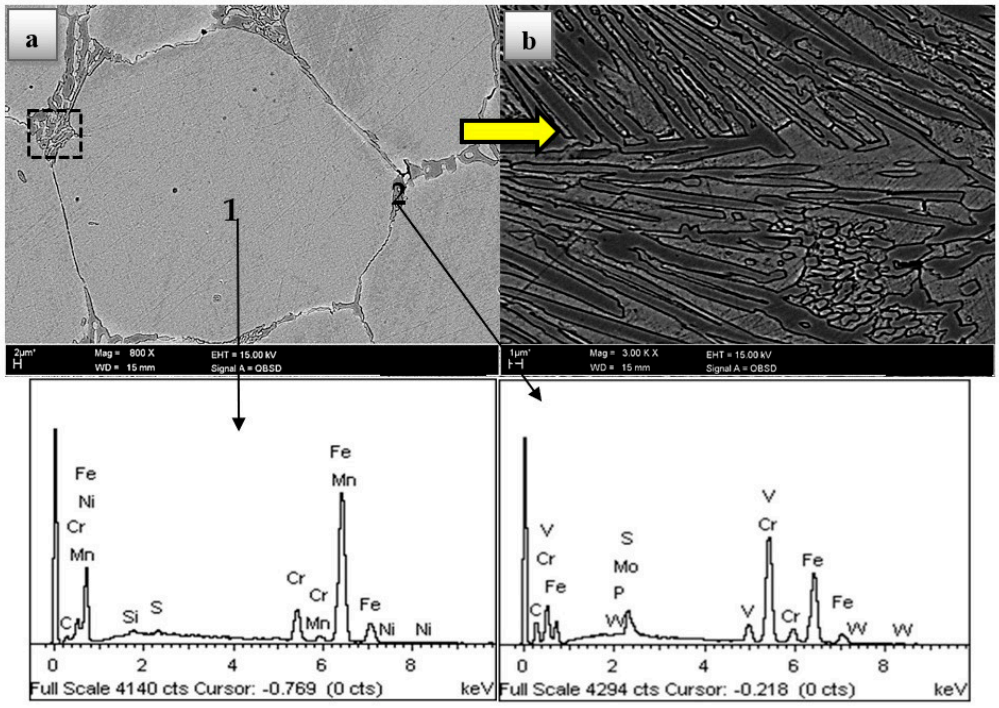


**Figure 13.** Top: SEM microstructure of partially remelted AISI D2 specimen at 1300 °C and bottom: analysis of EDX for points 1 and 2 where (**a**) area contains (**b**) which is an illustration of the dark rectangle.

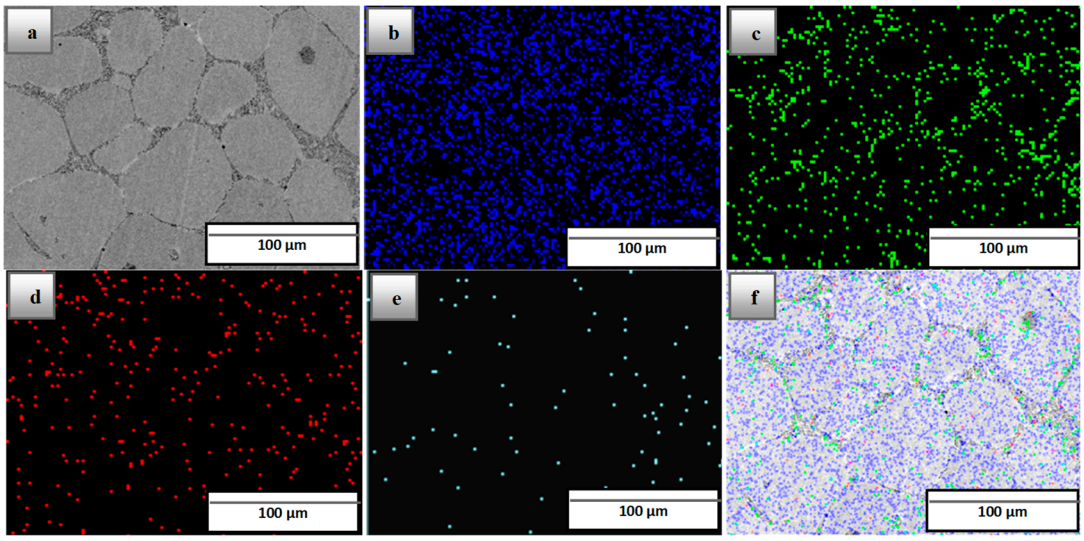


**Figure 14.** Findings of elemental mapping (SEM-EDX) of D2 tool steel:(**a**) SEM micrograph, (**b**) Fe, (**c**) Cr, (**d**) C, (**e**) V and (**f**) all four elements.

In order to determine the phase change and the varieties of carbide produced following direct partial remelting, X-ray diffraction (XRD) investigation was also carried out. Figure 15 shows the as-received tool steel's X-ray diffraction patterns both before and after heat treatment. As-received tool steel's diffraction patterns were examined, and peaks corresponding to the ferrite phase and iron–chromium carbide were discovered ($M_7C_3$). Following the application of the DPRM, the tool steel's XRD pattern shows three major phases involved within the matrix: ferrite, austenite, and $M_7C_3$. The primary link between the presence of austenite and an increase in C and Cr weight percentage in the solid solution is the stability of $\gamma$ [29]. Higher concentrations of these elements considerably impact the

temperature of martensite, making the conversion of austenite to martensite particularly challenging. Additionally, the austenitic phase is substantially more stable at ambient temperature when relatively quick cooling from the solidus–liquidus range is used [34].

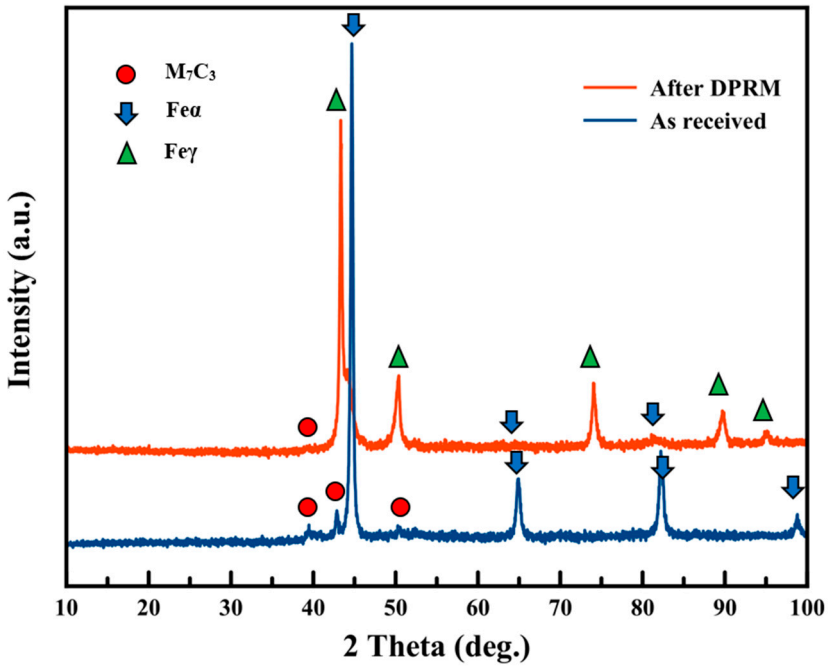


**Figure 15.** XRD pattern of as-received AISI D2 tool steel before and after DPRM at 1300°C.

### *3.4. Mechanical Properties*

After DPRM at 1300 °C, the hardness of AISI D2 was measured and was reported to be around 350 Hv, which is harder than the received tool steel with a hardness of 220 Hv. This suggests a phase transformation has taken place from ferrite and carbides to metastable austenite [32,34]. The post-DPRM microstructure of the D2 is particularly attractive because their mechanical and physical properties are more closely pertaining to the dissolved alloying components and precipitated carbides in ledeburite steel.

Figure 16 presents the results of the ultimate tensile strength of the as-received material after DPRM at 1300 °C samples. It is interesting to note that the AISI D2 tool steel, after exposure to the DPRM condition, exhibits a significant improvement (961MPa) over the as-received condition (791 MPa). This higher tensile strength obtained in the heat-treated condition is ascribed to the transformation of ferrite and carbides to metastable austenite, as well as the dissolution part of the eutectic chromium carbides in the matrix that changed the microstructure. However, it can be clearly seen that the fractures were characterised by brittleness with only 9% fracture strain if compared to the as-received condition (21%). The coarse fracture surface, which surprisingly displays some enormous solid lumps typical of the unbroken structure already discussed, is associated with brittleness.

Figure 17 displays the SEM fracture surface of the tensile fractured specimens of (a) the as-received material and (b) after DPRM at 1300 °C. It is clear that the mechanical properties of the globular microstructure of the specimens are somewhat better than those of the as-received material. As can be seen in Figure 17a, there are two types of small, spheroidized carbides and big carbides in a ferrite matrix. Due to the high carbon and high chromium content of D2, coarse chromium carbides are present throughout the matrix. Moreover, the fracture morphology in the fractrograph of Figure 17a shows that the carbide particle is separated into two pieces without experiencing plastic deformation. However, there is a plastically deformed region surrounding the carbide particle, evidenced by the appearance of many microvoids. Nevertheless, the fracture surface shows a mixed fracture mode of a ductile fracture along the matrix and a transgranular quasi-cleavage fracture in

the $M_7C_3$ carbides. The tensile fractured surfaces after DPRM have a different morphology than the as-received samples, as can be seen in Figure 17b. The fractures exhibit typical brittle characteristics, which illustrate the intergranular (typically dimpled) fracture mode. The micrographs reveal that the grain boundaries serve as the path of intergranular fracture and the liquidus–solidus interface, as shown in Figure 17b right [14]. The brittleness is related to the coarse fracture surface, which exhibits some surprisingly large solid lumps that are typical of the unbroken structure already mentioned.

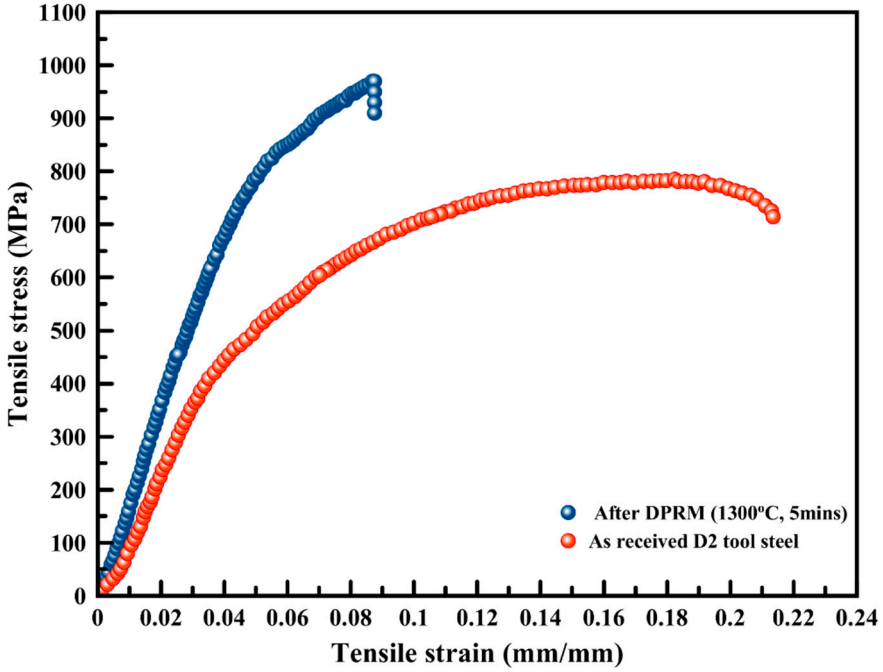


**Figure 16.** Stress–strain for as-received AISI D2 tool steel before and after DPRM at 1300 °C.

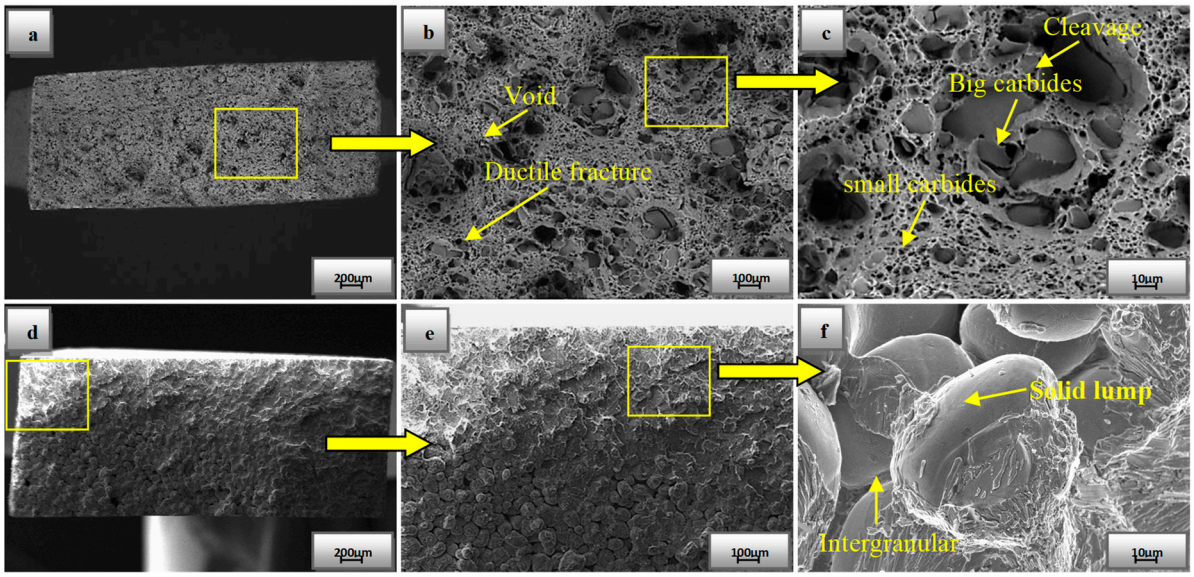


**Figure 17.** SEM fractography of: (**a**) as-received D2 with zoom-in zone (**b**,**c**) and (**d**) globular microstructure with zoom-in zone (**e**,**f**) of D2 after DPRM at 1300 °C.

## 4. Conclusions

The feasibility of the DPRM method for the fabrication of AISI D2 stock with a homogeneous globular structure was validated. The microstructural and mechanical

properties of D2 tool steel in the as-received annealed as well as semisolid conditions were also investigated. The following conclusions are summarized:

(1) Reheating into the semisolid region in the DPRM process supplied sufficient interfacial energy for the grain boundaries of the recrystallized structure to grow, while the presence of carbides prevented excessive grain size. The penetration of liquid towards grain boundaries is facilitated and promoted with a high eutectic volume fraction during the liquation process.
(2) Increasing the isothermal heating temperature makes the liquid phase distribute, surround the grain boundaries, and disperse more equally to produce globular grain. Globular-shaped grains are considered as an essential requirement for successful thixoforming. Therewith, most of original carbides were dissolved with increasing heating temperature while new eutectic carbides were re-precipitated along grain boundaries during subsequent cooling by diffusing carbide-forming elements into the grain boundaries
(3) The solid-state transformations above the eutectoid temperature at 1300 °C consisted mainly of the solid $\gamma$ phase, while cooling down from 1300 °C temperature results initially in the transformation of the remaining liquid into eutectic ($L \rightarrow \gamma + M_7C_3$). It is well known that maintaining stable austenite against transformation to martensitic at low temperatures relies on the alloying element concentration in the material, especially on the carbon and chromium.
(4) Metastable austenite transformation contributes to the enhancement of AISI D2 mechanical properties. Where they increased after the application of a direct partial remelting (hardness of 220 Hv to 350 Hv, tensile strength of 791 MPa to 961 MPa). The fracture surfaces after DPRM exhibited a different morphology compared to the as-received samples; the former showed an intergranular (typically dimple) fracture mode along the liquidus–solidus contact and grain boundaries.

**Author Contributions:** M.N.M. and M.Z.O. conceived and designed the experiments; A.N.J.A.-T., H.S.S. and L.H.A. performed the experiments; S.A.-Z., O.I.A. and M.A. wrote the original paper and analyzed the results. All authors have read and agreed to the published version of the manuscript.

**Funding:** Universiti Kebangsaan Malaysia (UKM) and the Ministry of Higher Education (MoHE), Malaysia, Research Grant sv AP-2012-014.

**Institutional Review Board Statement:** Not applicable.

**Informed Consent Statement:** Not applicable.

**Data Availability Statement:** The study did not report any data.

**Acknowledgments:** The authors would like to thank Universiti Kebangsaan Malaysia (UKM) and the Ministry of Higher Education (MoHE), Malaysia.

**Conflicts of Interest:** The authors declare no conflict of interest.

## References

1. Meng, Y.; Sugiyama, S.; Yanagimoto, J. Microstructural evolution during RAP process and deformation behavior of semi-solid SKD61 tool steel. *J. Mater. Process. Technol.* **2012**, *212*, 1731–1741. [CrossRef]
2. Spencer, D.B.; Mehrabian, R.; Flemings, M.C. Rheological behavior of Sn-15 pct Pb in the crystallization range. *Met. Mater. Trans.·A* **1972**, *3*, 1925–1932. [CrossRef]
3. Fan, Z. Semisolid metal processing. *Int. Mater. Rev.* **2002**, *47*, 49–85. [CrossRef]
4. Salleh, M.S.; Omar, M.Z.; Syarif, J.; Alhawari, K.S.; Mohammed, M.N. Microstructure and mechanical properties of thixoformed A319 aluminium alloy. *Mater. Des.* **2014**, *64*, 142–152. [CrossRef]
5. Mohammed, M.N.; Omar, M.Z.; Sajuri, Z.; Salleh, M.S.; Alhawari, K.S. Trend and Development of Semisolid Metal Joining Processing. *Adv. Mater. Sci. Eng.* **2015**, *2015*, 846138. [CrossRef]
6. Alhawari, K.S.; Omar, M.Z.; Ghazali, M.J.; Salleh, M.S.; Mohammed, M.N. Evaluation of the microstructure and dry sliding wear behaviour of thixoformed A319 aluminium alloy. *Mater. Des.* **2015**, *76*, 169–180. [CrossRef]
7. Arif, M.A.M.; Omar, M.Z.; Muhamad, N.; Syarif, J.; Kapranos, P. Microstructural Evolution of Solid-solution-treated Zn–22Al in the Semisolid State. *J. Mater. Sci. Technol.* **2013**, *29*, 765–774. [CrossRef]

8. Eugênio José Zoqui, A.S.R. Hipólito Domingo Carvajal Fals: Microstructure of Thixoformable Hypoeutectic Cast Iron. *Solid State Phenom.* **2012**, *192–193*, 219–224.
9. Mohammed, M.N.; Omar, M.Z.; Salleh, M.S.; Alhawari, K.S. Study on Thixojoining Process Using Partial Remelting Method. *Adv. Mater. Sci. Eng.* **2013**, *2013*, 251472. [CrossRef]
10. Roca, A.S.; Fals, H.D.C.; Pedron, J.A.; Zoqui, E.J. Thixoformability of hypoeutectic gray cast iron. *J. Mater. Process. Technol.* **2012**, *212*, 1225–1235. [CrossRef]
11. Omar, M.Z.; Atkinson, H.V.; Kapranos, P. Thixotropy in Semisolid Steel Slurries under Rapid Compression. *Met. Mater. Trans. A* **2011**, *42*, 2807–2819. [CrossRef]
12. Uhlenhaut, D.I.; Kradolfer, J.; Püttgen, W.; Löffler, J.F.; Uggowitzer, P.J. Structure and properties of a hypoeutectic chromium steel processed in the semi-solid state. *Acta Mater.* **2006**, *54*, 2727–2734. [CrossRef]
13. Püttgen, W.; Hallstedt, B.; Bleck, W.; Löffler, J.F.; Uggowitzer, P.J. On the microstructure and properties of 100Cr6 steel processed in the semi-solid state. *Acta Mater.* **2007**, *55*, 6553–6560. [CrossRef]
14. Meng, Y.; Sugiyama, S.; Soltanpour, M.; Yanagimoto, J. Effects of predeformation and semi-solid processing on microstructure and mechanical properties of Cr–V–Mo steel. *J. Mater. Process. Technol.* **2013**, *213*, 426–433. [CrossRef]
15. Li, J.-Y.; Sugiyama, S.; Yanagimoto, J. Microstructural evolution and flow stress of semi-solid type 304 stainless steel. *J. Mater. Process. Technol.* **2005**, *161*, 396–406. [CrossRef]
16. Omar, M.Z.; Alfan, A.; Syarif, J.; Atkinson, H.V. Microstructural investigations of XW-42 and M2 tool steels in semi-solid zones via direct partial remelting route. *J. Mater. Sci.* **2011**, *46*, 7696–7705. [CrossRef]
17. Wang, Y.; Bi, S.; Song, R.; Yanagimoto, J.; Taylor, T. Extremely high temperature carbide precipitation induced intragranular acicular ferrite transformation of M2 steel during semi-solid cooling. *Mater. Lett.* **2022**, *310*, 131516. [CrossRef]
18. De Freitas, C.C.; Caram, R.; Campo, K.N. Semisolid deformation behavior and processing of CoCrCuxFeNi high-entropy alloys. *Intermetallics* **2022**, *150*, 107682. [CrossRef]
19. Chang, Z.; Wang, X.; Wu, Y.; Peng, L.; Ding, W. Review on criteria for assessing the processability of semisolid alloys. *Mater. Lett.* **2020**, *282*, 128835. [CrossRef]
20. Mohammed, M.N.; Omar, M.Z.; Salleh, M.S.; Alhawari, K.S.; Kapranos, P. A Study of Microstructure Properties of AISI D2 Tool Steel in Partial Re-Melting Method. *Appl. Mech. Mater.* **2014**, *699*, 76–80. [CrossRef]
21. Mohammed, M.N.; Omar, M.Z.; Salleh, M.S.; Alhawari, K.S.; Kapranos, P. Semisolid Metal Processing Techniques for Nondendritic Feedstock Production. *Sci. World J.* **2013**, *2013*, 752175. [CrossRef] [PubMed]
22. Jirková, H.; Rubešová, K.; Konopík, P.; Opatová, K. Effect of the Parameters of Semi-Solid Processing on the Elimination of Sharp-Edged Primary Chromium Carbides from Tool Steel. *Metals* **2018**, *8*, 713. [CrossRef]
23. Meengam, C.; Sillapasa, K. Evaluation of Optimization Parameters of Semi-Solid Metal 6063 Aluminum Alloy from Friction Stir Welding Process Using Factorial Design Analysis. *J. Manuf. Mater. Process.* **2020**, *4*, 123. [CrossRef]
24. Nakowong, K.; Sillapasa, K. Optimized Parameter for Butt Joint in Friction Stir Welding of Semi-Solid Aluminum Alloy 5083 Using Taguchi Technique. *J. Manuf. Mater. Process.* **2021**, *5*, 88. [CrossRef]
25. Ritter, E.P.; Stumpf, F.T. Finite-element simulation of semi-solid metal processing of tool steel encased in carbon steel. *Simulation* **2022**, *98*, 563–574. [CrossRef]
26. Binesh, B.; Aghaie-Khafri, M.; Shaban, M.; Fardi-Ilkhchy, A. Microstructural Evolution and Mechanical Properties of 7075 Aluminium Alloy during Semi-Solid Compression Deformation. *Crystals* **2022**, *12*, 1119.
27. Hirt, G.; Khizhnyakova, L.; Baadjou, R.; Knauf, F.; Kopp, R. Semi-Solid Forming of Aluminium and Steel–Introduction and Overview. In *Thixoforming*; Wiley-VCH GmbH & Co. KGaA: Aachen, Germany, 2019; pp. 1–27.
28. Bombac, D.; Fazarinc, M.; Podder, A.S.; Kugler, G. Study of Carbide Evolution During Thermo-Mechanical Processing of AISI D2 Tool Steel. *J. Mater. Eng. Perform.* **2013**, *22*, 742–747. [CrossRef]
29. Püttgen, W.; Hallstedt, B.; Bleck, W.; Uggowitzer, P.J. On the microstructure formation in chromium steels rapidly cooled from the semi-solid state. *Acta Mater.* **2007**, *55*, 1033–1042. [CrossRef]
30. Mohammed, M.N.; Omar, M.Z.; Syarif, J.; Sajuri, Z.; Salleh, M.S.; Alhawari, K.S. Microstructural Evolution during DPRM Process of Semisolid Ledeburitic D2 Tool Steel. *Sci. World J.* **2013**, *2013*, 1–7. [CrossRef]
31. Omar, M.Z.; Atkinson, H.V.; Howe, A.A.; Palmiere, E.J.; Kapranos, P.; Ghazali, M.J. Solid–liquid structural break-up in M2 tool steel for semi-solid metal processing. *J. Mater. Sci.* **2009**, *44*, 869–874. [CrossRef]
32. Mohammed, M.N.; Omar, M.Z.; Syarif, J.; Salleh, M.S. Morphological evolution during partial re-melting of AISI D2 Cold-Work Tool Steel. *Sains Malays.* **2014**, *43*, 1213–1219.
33. Bhadeshia, H.; Honeycombe, R. *Steels: Microstructure and Properties*, 3rd ed.; Butterworths-Heinemann: Cambridge, UK, 2006.
34. Aisman, D.; Jirkova, H.; Kucerova, L.; Masek, B. Metastable structure of austenite base obtained by rapid solidification in a semi-solid state. *J. Alloys Compd.* **2011**, *509* (Suppl. 1), S312–S315. [CrossRef]